Progress In Electromagnetics Research C, Vol. 138, 1–12, 2023

Structural and Electromagnetic Shielding Effectiveness of Carbon-Coated Cobalt Ferrite Nanoparticles Prepared via Hydrothermal Method

Nur Amirah Athirah binti Zaini, Iffah Zulaikha binti Azman, Ling Jin Kiong, Jose Rajan, Muhammad Hafiz Mazwir, and Mohamad Ashry Jusoh*

Abstract—The rapid advancement of communication technology has led to an increase in electromagnetic interference (EMI), or electromagnetic (EM) pollution. This is a cause for concern, as EMI can disrupt communication services, damage electronic equipment, and pose health risks. Regulatory bodies are working to develop standards for the safe use of wireless devices, but the problem of EMI is likely to continue to grow as the number of Internet of Thing (IoT) devices continues to increase. To address this issue, this study investigated the effectiveness of carbon-coated cobalt ferrite nanoparticles as a potential material for electromagnetic shielding. The synthesis of cobalt ferrite ($CoFe_2O_4$) nanoparticles was successfully achieved using the co-precipitation method. Subsequently, a carbon coating was applied to the nanoparticles through a hydrothermal process using a 200 mL autoclave made of teflon-lined stainless steel. This process was carried out at a temperature of 180°C for a duration of 12 hours, with a heating rate of 8°C per minute. This study examined both uncoated and carbon-coated $CoFe_2O_4$ nanoparticles at various ratios of glucose to $CoFe_2O_4$ ($1:1, 2:1$, and $3:1$) using techniques such as X-ray diffraction (XRD), field emission scanning electron microscopy (FESEM), and higher resolution transmission electron microscopy (HRTEM) analysis. The XRD analysis revealed distinct and well-defined peaks corresponding to $CoFe_2O_4$, indicating the successful synthesis of the nanoparticles. The crystallite size of the uncoated $CoFe_2O_4$ nanoparticles was measured to be 11.47 nm, while for the carbon-coated $CoFe_2O_4$, the average crystallite size was determined to be 14.15 nm through XRD analysis. The results obtained from the FTIR analysis were consistent with previous reports and confirmed the formation of spinel $CoFe_2O_4$ nanoparticles, as suggested by published data. The morphological and structural properties of the prepared samples were further characterized using FESEM and HRTEM analysis, which demonstrated uniformity in both particle size distribution and morphology. Overall, the research findings indicated that the structure and properties of $CoFe_2O_4$ nanoparticles were significantly influenced by the carbon coating process. Notably, the optimum ratio of carbon to $CoFe_2O_4$ was found to be $2:1$, which resulted in the highest carbon thickness. The electromagnetic properties of the samples were evaluated using a vector network analyzer (VNA) and measured S-parameters in the frequency range of 8.2 to 12.4 GHz, known as the x-band region, suitable for radar applications. The sample with a carbon ratio of $2:1$ exhibited the highest total shielding effectiveness (SE) of 17 dB at approximately 10 GHz. As a conclusion, the carbon-coated $CoFe_2O_4$ nanoparticles showed promising potential as an effective material for shielding against electromagnetic wave pollution, particularly when the carbon coating and filler composition reached an optimal point. Additionally, the shielding effectiveness performance of the sample could be further enhanced by incorporating a conductive polymer as an auxiliary material.

Received 23 February 2023, Accepted 19 July 2023, Scheduled 19 September 2023

* Corresponding author: Mohamad Ashry Jusoh (ashry@ump.edu.my).

The authors are with the Faculty of Industrial Sciences & Technology, Universiti Malaysia Pahang, Gambang, Pahang 26300, Malaysia.

1. INTRODUCTION

Among the elements in the period table, transition metal oxides nanostructures are the class of magnetic materials that have been extensively used in many applications in the past decades. The spinel ferrite structure with the formula of M-Fe_2O_4 where M could be Co, Ni, Zn, or other metals can be described as a cubic closely packed arrangement of oxygen atoms, and M^{2+} and Fe^{3+} ions can occupy either tetrahedral (A) or octahedral (B) sites. Electronic, magnetic, and catalytic properties have been attracting the usage of spinel ferrite nanoparticles in research. Among the spinel ferrites, cobalt ferrite ($CoFe_2O_4$) however has an inverse spinel structure in which in the ideal state, all Co^{2+} ions are in B sites, and Fe^{3+} ions are equally distributed between A and B sites. The advantages of having $CoFe_2O_4$ itself are due to its high coercivity, high electromagnetic performance, mechanical hardness, excellent chemical stability, and moderate saturation magnetization whose result gives a good candidate for the electronic components used in computers, recording devices, and shielding materials. As such cobalt ferrite is used in the biomedical field for magnetic resonance imaging (MRI) due to its high magnetic anisotropy and moderate magnetization based on a study by Wang et al., 2016 [1].

Moreover, Co and Fe are magnetic materials that can be used as a base to grow carbon-based materials as they serve as sites for nucleation and growth. The combination of these two kinds of materials has greatly contributed to the production of composites. Nanocomposite fabrication has become a major area of research and development owing to the remarkable properties and multifunctional behaviours derived from their nanocomposite structure itself. Magnetic polymer nanocomposite is one of the special interests due to the combination of excellent magnetic properties, high specific area, surface active sites, high chemical stability, and good compatibility. In another study, it is also found that the GO nanosheets were coated by cobalt ferrite nanoparticles which are densely deposited on both sides of the GO nanosheets to form a sandwich-like composite structure [1]. While according to research on oil recovery application, the coating process for cobalt ferrite nanoparticles on the surface of GO nanosheets was efficient and homogeneously decorated using the facile sonochemical method where the presence of it improves the oil recovery in terms of magnetic field strength [2].

To have these properties, it is highly influenced by the chemical composition and microstructural characteristics, which can be controlled during the fabrication and synthesis method. Many chemical routes have been already adopted by many researchers to synthesise the nanoparticles of $CoFe_2O_4$ such as the sol-gel method [3], co-precipitation [4], and electrospinning [5]. Consequently, the preparation of cobalt ferrite nanoparticles through different routes has become one of the important areas in research and development. As proved, there are many studies for the synthesis and fabrication of $CoFe_2O_4$ nanostructures in many forms of composites such as fibre [5], sheets [1], and particles [2]. Among the other synthetic methods, the hydrothermal method is a better alternative with some of its advantages of simplicity, low cost, high purity, controllable thickness of the coating, and low environmental pollution due to the no usage of any harmful organic solvent for biohazards inactivation [6].

Electromagnetic interference (EMI) is one of the electromagnetic wave pollutions over a frequency range that affects and degrades the performance of devices which may be caused by electromagnetic coupling, electromagnetic induction, or conduction. The EMI not only affects the devices but also threatens human health such as the cardiovascular and nervous systems [7]. The basic concept of shielding itself is to isolate the electrical devices from their surrounding wave pollution. Epoxy-based composites are emerging in the shielding of electromagnetic interference in comparison to conventional materials. It is due to the advantages and excellent properties such as lightweight structure, chemical and heat stability, antibacterial properties, low contractibility, strong adherence, good dielectric constant, low shrinkage, and favourable strength to the weight where mechanical properties are extremely important for structural applications [8].

In the present study, carbon-coated $CoFe_2O_4$/epoxy nanocomposite was synthesised from an aqueous solution containing metal nitrates using a hydrothermal method followed by calcination for the carbon coating. This method does not require the addition of any other chemicals to the solution, and it has the advantages of simplicity, low cost, no by-product at all, and an environmentally friendly operation. The textural and morphological characteristics of the prepared $CoFe_2O_4$ were studied with various techniques to verify the particle size and distribution as well as to explore other parameters of interest. The composite is further fabricated using epoxy as the polymer and shielding effectiveness by having its conductivity, permittivity, and permeability by using the vector network analyser.

2. EXPERIMENTAL METHODS AND MATERIALS

Cobalt nitrate hexahydrate (Co $(NO_3)_{2.6}H_2O$) with a molecular weight of 291.03 g/mol and ferrite nitrate nano hydrate (Fe $(NO_3)_{3.9}H_2O$) with a molecular weight of 404.00 g/mol was purchased from Sigma Aldrich, United Kingdom. Acetone ($C_3H_6O_7$), sodium chloride (NaCl), and sodium hydroxide (NaOH) were purchased from Merck, Germany. All the chemicals and materials were used without further purification. Deionized distilled water was used throughout all experiments. The synthesis was carried out with a hydrothermal reaction using a 200 mL autoclave Teflon-lined stainless steel.

2.1. Synthesis of $CoFe_2O_4$ Nanoparticle

The synthesis was carried out with a hydrothermal reaction of a stoichiometric mixture of the reagents. Typically, 2.286 g of cobalt nitrate and 6.046 g of ferrite nitrate were used as the precursor of the sample. These raw materials were dissolved in an aqueous deionized solution of 250 mL, and the solutions were stirred separately at 250 rpm until fully dissolved and then were mixed into one solution. The mixed solutions were stirred for another few minutes to get a homogenous mixture and then heated up gradually up to 70°C until the dark solution was formed. Then, 0.8 M of NaOH was added by drop until the pH of 9 is reached under rigorously stirring in a magnetic stirrer with a hot plate. The mixture was transferred to a 200 mL Teflon-lined stainless-steel autoclave and heated in the oven where the temperature was increased from 25 to 180°C at a rate of $8°C\,min^{-1}$ and maintained for 10 h. The autoclave was then cooled to room temperature ($\sim 25°C$). The resulting dark grey product was filtered with a membrane filter of 0.45 μm Millipore. The product was then washed thoroughly several times with deionized water and ethanol alternately and finally dried at 60°C for 12 h. Finally, it was dried in a programmed oven at 100°C for 12 h. Next, the dried sample was crushed to obtain fine particles using mortar and pestle, and $CoFe_2O_4$ nanoparticles are obtained.

2.2. Synthesis of Carbon-Coated $CoFe_2O_4$ Nanoparticle

The obtained $CoFe_2O_4$ was then further used to be coated with carbon in the presence of glucose with a controllable thickness. The $CoFe_2O_4$ was dispersed in the glucose of 50 ml solution where the ratio of glucose to $CoFe_2O_4$ was 1 : 2. The mixed solution was transferred to Teflon lined autoclave and kept at 150°C for 12 h. After the completion of the reaction, the final product was washed several times with distilled water and ethanol alternately. Then it was dried at 100°C for 12 h in an oven. The resultant powder was carbonized at 450°C for 3 h under an argon atmosphere to obtain the carbon-coated $CoFe_2O_4$. The carbon-coated $CoFe_2O_4$ was prepared by varying the ratio of glucose to $CoFe_2O_4$ $(1:2, 2:1, 3:1)$ using the same procedures. The samples were accordingly denoted as C/$CoFe_2O_4$ — 1, C/$CoFe_2O_4$ — 2 and C/$CoFe_2O_4$ — 3.

2.3. Fabrication of Nanocomposite Carbon-Coated $CoFe_2O_4$/Epoxy

The carbon-coated $CoFe_2O_4$ was further used in the fabrication of nanocomposite using epoxy resin as the matrix. The carbon-coated $CoFe_2O_4$ was mixed with epoxy and hardener in a ratio of 1 : 1. The filler was mixed with the mixture of epoxy resin via syringe, then by followed by using a dropper and mini mechanical vortex for 15 minutes until a homogenous mixture was obtained. Then the mixture was poured slowly into X-band mold with dimension 22.86 mm × 10.16 mm × 2 mm to avoid bubble forming. The sample was allowed to cure in the atmosphere for 48 hours.

The graphical methodology of synthesizing cobalt ferrite, carbon-coated cobalt ferrite, and composite fabrication were illustrated in Fig. 1.

3. CHARACTERIZATION TECHNIQUES

The morphology and grain size of the particles were measured by FESEM (model JSM008F), and the images were taken at 10x magnification to 100x magnification. The structure of the $CoFe_2O_4$ nanoparticles was characterized by the XRD technique (model Rigaku Corporation, Japan) using Cu Kα radiation (0.154 nm) operating at 40 mA and 40 kV to generate diffraction patterns from the crystalline

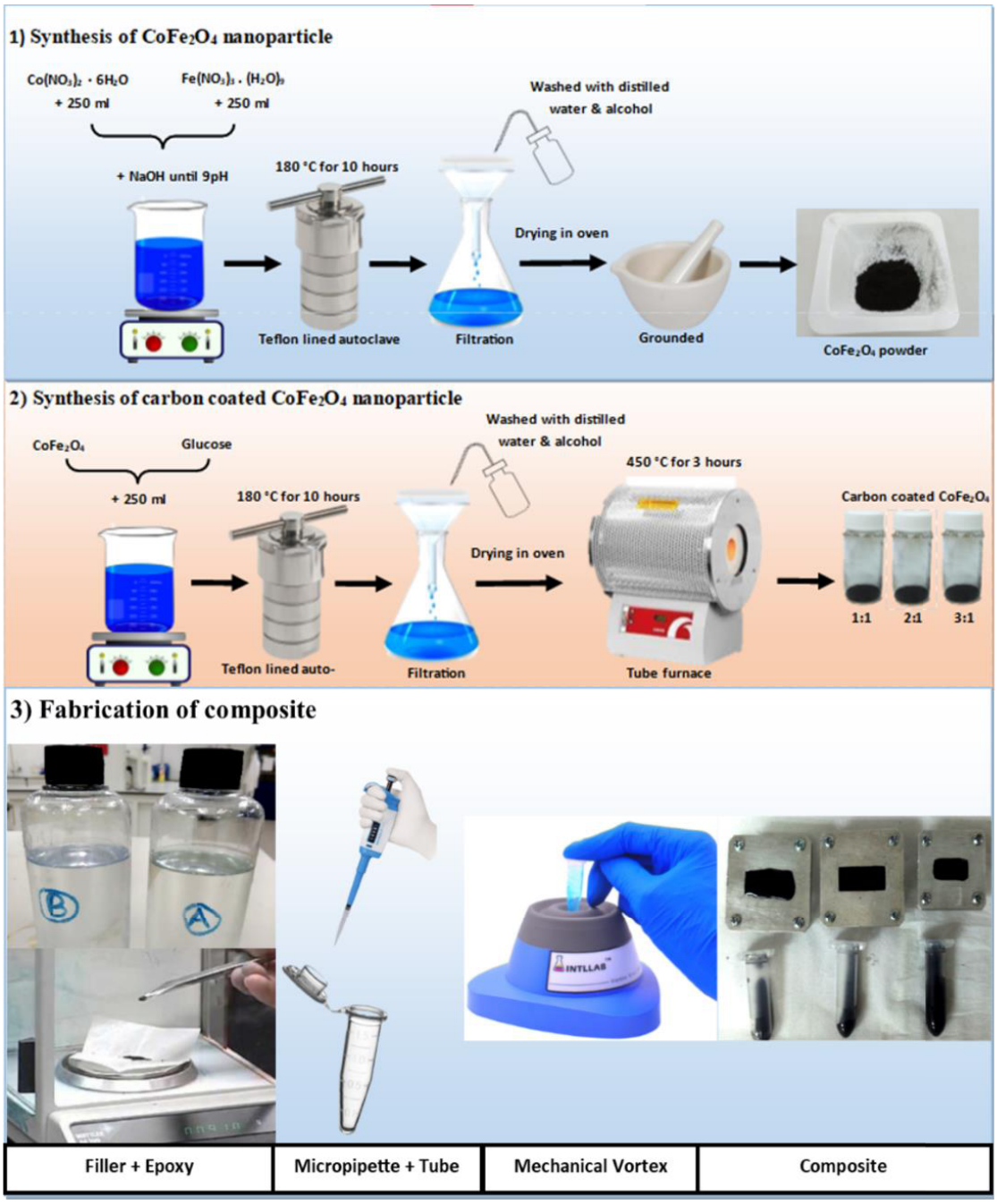

Figure 1. Steps in synthesising the carbon-coated $CoFe_2O_4$/epoxy composite.

powder samples at ambient temperature over the 2θ range from 10° to 80°. Infrared spectra from 400 to 4000 cm^{-1} were recorded using an FT-IR spectrometer (model Perkin Elmer 100) with the samples ground with KBr and compressed into a pellet, and the signal was detected in transmittance mode (%T). The selected areas were obtained from the samples to ascertain both morphologies, carbon thickness, and particle size distribution at different ratios of carbon coating by high-resolution transmission electron microscopy (model JEOL JEM 2100F) operating at an accelerating voltage of 200 kV. All together the XRD, HRTEM, FESEM, and FTIR results were used to establish the crystallinity of the prepared $CoFe_2O_4$ powder at different ratios of carbon coating.

3.1. Shielding Effectiveness Characterization

A Keysight E5071C Vector Network Analyser (VNA) was used to measure the reflection coefficient, S_{11}, and transmission coefficient, S_{21} at X-band frequency from 8.2 GHz to 12.4 GHz. The samples were carefully poured into an X-band mold as shown in Fig. 2(a), ensuring a precise placement and no bubble trapped. The mold was specifically designed to accommodate the samples, providing a suitable environment for their containment. To facilitate the measurement process, the specimens were then inserted between two rectangular X-band waveguides, creating a sandwich-like configuration as shown in Fig. 2(b). This arrangement allowed for efficient transmission of electromagnetic waves through the samples, facilitating accurate data collection and analysis. To minimize measurement errors, the Vector Network Analyzer (VNA) used in the study was calibrated using a full-2 port calibration technique. This calibration was performed at the end of the waveguide adapter which is known as calibration plane. The shielding effectiveness was calculated based on the scattering parameters (S_{11} and S_{21}) obtained from two-port reflection/transmission measurement using VNA as shown in Fig. 2(c). The shielding effectiveness is the total of electromagnetic shielding due to reflection, SE_R, and absorption, SE_A as express in Eqs. (1)–(3) [9, 10].

$$\mathrm{SE}_R\,(\mathrm{dB}) = 10\log_{10}\left(\frac{1}{1-|S_{11}|^2}\right) \tag{1}$$

$$\mathrm{SE}_A\,(\mathrm{dB}) = 10\log_{10}\left(\frac{1-|S_{11}|^2}{|S_{21}|^2}\right) \tag{2}$$

$$\mathrm{SE}_{\mathrm{Total}}\,(\mathrm{dB}) = \mathrm{SE}_R + \mathrm{SE}_A \tag{3}$$

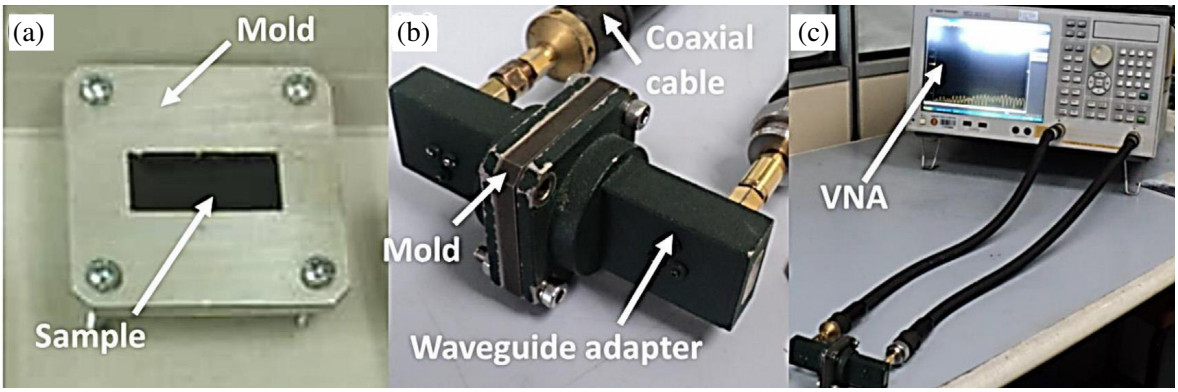

Figure 2. Electromagnetic shielding effectiveness measurement. (a) Sample composite in the X-band sample holder, (b) sample is attached to sample holder while connected to waveguide adapters, and (c) two-port reflection/transmission setup of Keysight E5071C VNA.

4. RESULTS AND DISCUSSIONS

4.1. X-Ray Diffraction (XRD)

Figure 3 shows the XRD patterns of the different samples ratio and $CoFe_2O_4$ nanoparticle. The highly intense and sharp diffraction peaks show that the metal oxide is of high purity which confirms the presence of $CoFe_2O_4$ with a face-centred cubic structure [11]. Besides, no other phases were detected other than those that belong to $CoFe_2O_4$, indicating that the sample is free from impurity. Specifically, the diffraction peaks at 18.24°, 3.06°, 3.45°, 3.28°, 4.47°, 5.89°, 5.17°, 6.73°, 6.70°, 7.79°, 7.00°, 7.38°, and 79.08° can be indexed to the (111), (220), (311), (222), (400), (422), (511), (440), (531), (620), (533), (622), and (444), crystals planes of $CoFe_2O_4$ phases with an *Fd3m* space group.

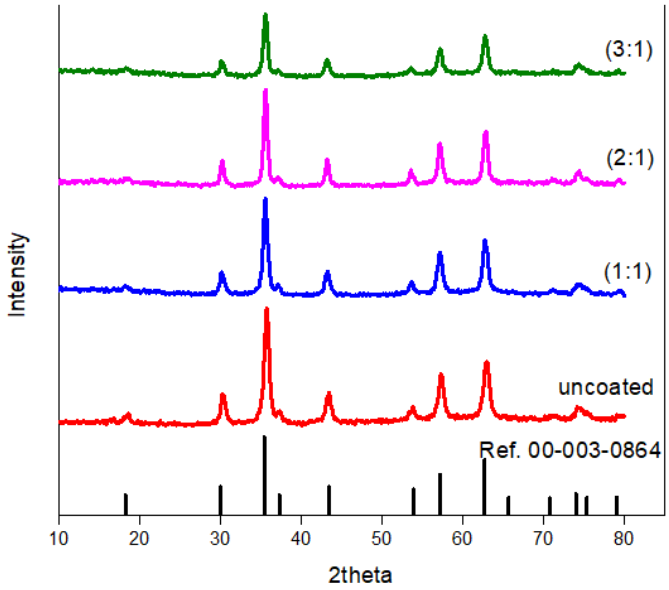

Figure 3. XRD pattern of $CoFe_2O_4$ nanoparticles and the ratio of glucose to $CoFe_2O_4$ at (1 : 1), (2 : 1) and (3 : 1).

The results show that, as the carbon coating decreases, the diffraction peaks become sharper and narrower, and their intensity increases. This indicates an intensification in crystallinity that originates from the increment of crystalline volume ratio due to the particle size enlargement of the nuclei. The higher content of ratio refers to the higher content of carbon revealed by the broad peak and indicates that the sample is amorphous. The average crystallite size was also determined from the full width at the half maximum (FWHM) of the XRD patterns, using the well-known Scherer formula:

$$D = 0.9\frac{\lambda}{\beta}\cos\theta \tag{4}$$

where D is the crystallite size (nm); β is the full width of the diffraction line at half of the maximum intensity measured in radians; λ is the X-ray wavelength of Cu Kα = 0.154 nm; and θ is the Bragg angle [12]. The crystallite sizes estimated using the Scherer formula were found to increase with the increase in the ratio of carbon coating from 11.47 nm at ratio (0 : 1) to about 15.42 nm at ratio (2 : 1) as shown in Table 1 until it dropped at ratio (3 : 1).

Table 1. Average particle size and thickness of $CoFe_2O_4$ determined from XRD and HRTEM for the different ratios of carbon-coated $CoFe_2O_4$.

$CoFe_2O_4$ nanoparticles	**The ratio of carbon coating**	**Average crystallite size XRD (nm)**	**The thickness of carbon coating from HRTEM (nm)**
Uncoated	(0 : 1)	11.47	No coating
$CoFe_2O_4$ 1	(1 : 1)	12.92	1.13
$CoFe_2O_4$ 2	(2 : 1)	15.42	4.24
$CoFe_2O_4$ 3	(3 : 1)	14.11	1.59

4.2. Fourier Transform Infrared (FTIR)

The FTIR spectrum of carbon-coated $CoFe_2O_4$ is shown in Fig. 4 with a wavenumber between 400 and 4000 cm^{-1}. The FTIR spectrum describes the position of the ions in the crystal structure and their vibration modes. The two common bands in almost all spinel ferrite are found in the region of 400–600 cm^{-1}. The frequency bands around 606–616 and 421–430 cm^{-1} are assigned to the tetrahedral and octahedral clusters and also confirm the presence of Fe metal oxide (M-O) stretching vibration in $CoFe_2O_4$ nanoparticles [13]. To be specific, the appearance of a peak at 575 cm^{-1} is attributed to stretching vibrations of Fe^{3+}-O^{2-} which are observed in all ferrite samples and corresponds to Fe in the tetrahedral sites [14] while the peak at 631 cm^{-1} is due to the stretching vibrations mode associated with the metal-oxygen absorption band. The peaks at 600 and 450 cm^{-1} also represent the characteristics of Co_2O_3 [15]. The antisymmetric stretching, symmetric stretching, out-of-plane bending, and symmetric in-plane bending peaks of the cobalt metals are observed at 1629, 1388, 870, and 664 cm^{-1}, respectively [16]. The FTIR absorption bands of solids are usually assigned to the vibration of ions in the crystal lattice [17].

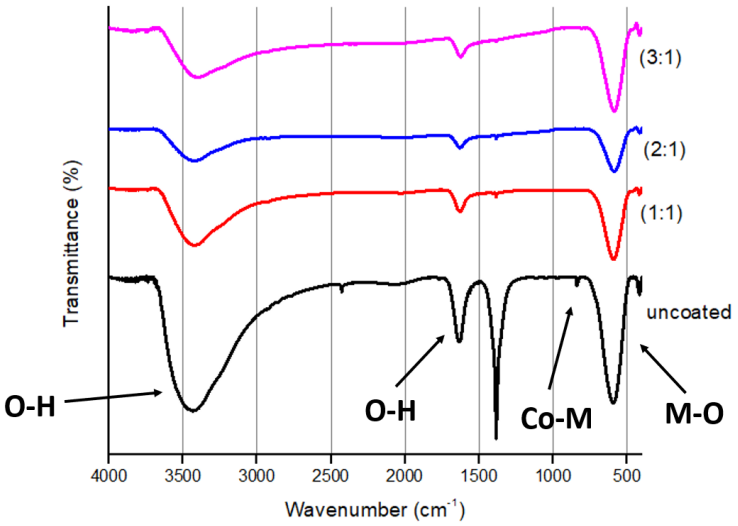

Figure 4. FTIR spectrum of $CoFe_2O_4$ nanoparticles and the ratio of glucose to $CoFe_2O_4$ at (1 : 1), (2 : 1) and (3 : 1).

The broad peak in the frequency range of 3450–3550 cm^{-1} is attributed to the O-H stretching vibration of the water molecules [18]. The absorption broadband at 3400 and 1620 cm^{-1} represents a stretching and bending mode of OH groups [3]. The transmittance intensity decreases drastically when the sample increases in carbon coating. This decrease is due to the loss of the residual water in the sample which shows a strong bonding between them. The obtained peaks are well matched with earlier reports and indicate the formation of the spinel $CoFe_2O_4$ nanoparticles as suggested by previously published data [11].

4.3. Field Emission Scanning Electron Microscopy (FESEM)

The morphology of $CoFe_2O_4$ and carbon-coated $CoFe_2O_4$ was observed by FESEM as shown in Fig. 5 as a result of the synthesized hydrotherma. The results indicate that the samples are uniform in both morphology and particle size distribution. The $CoFe_2O_4$ nanoparticles without carbon coating at 30 k magnification clearly showed a relatively large distribution of particles on average about 129 nm.

For all of the carbon-coated $CoFe_2O_4$ samples, it can be observed that the morphology did not give any significant difference between them, thus HRTEM is needed to define the coating further. As for crystalline $CoFe_2O_4$ nanoparticle, it is commonly accepted that their surface, similar to other iron oxide nanoparticles, is covered with a thin magnetically disordered shell of about 1 nm thickness [19].

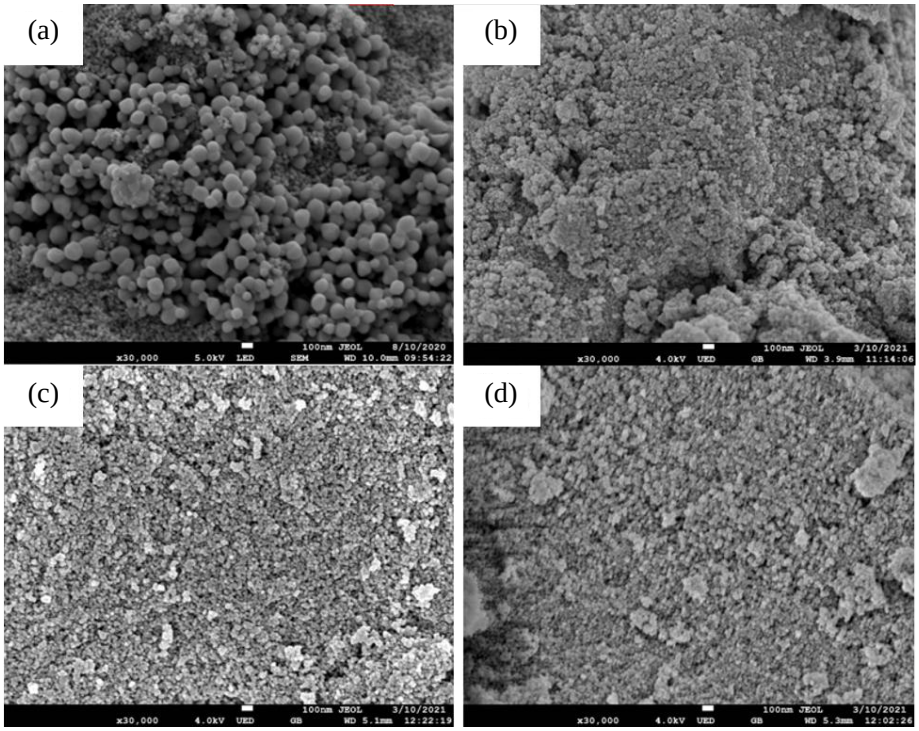

Figure 5. Field Emission Scanning Electron Microscope (FESEM) image of $CoFe_2O_4$, (a) uncoated $CoFe_2O_4$, (b) $C/CoFe_2O_4$ — 1, (c) $C/CoFe_2O_4$ — 2 and (d) $C/CoFe_2O_4$ — 3.

This phenomenon is attributed to the fact that carbon/glucose played a flexible confinement function to enwrap the $CoFe_2O_4$ nanoparticles which further prevented the particle from agglomerating [1]. The particle size increased with the increasing ratio of carbon coating which is in good agreement with the XRD results in Table 1 but dropped at ratio (2 : 1) to (3 : 1). The smallest particle size with carbon coating obtained in this study was 12.92 nm at a ratio (1 : 1), and particle size reached 1.11 nm at the highest ratio of carbon coating at (3 : 1). This suggests that several neighbouring particles fuse to increase the particle sizes by melting their surface. It is well known that particle size is crucial for many applications especially in biomedical development to be used inside the living system [20].

4.4. High-Resolution Transmission Electron Microscope (HRTEM)

Figure 6 shows the HRTEM images of carbon-coated $CoFe_2O_4$ nanoparticle. The carbon layers seemed to closely coat the $CoFe_2O_4$ nanoparticles which favoured the contact and charge transfer between them. No lattice fringe was found in the HRTEM image of carbon coating around the $CoFe_2O_4$ nanoparticles, further suggesting its amorphous phase.

It is worth noting that almost no free $CoFe_2O_4$ nanoparticles are observed outside the carbon coating, indicating a strong interaction between them. The possible formation mechanism of carbon over $CoFe_2O_4$ can be explained as follows. Initially, the uniform $CoFe_2O_4$ nanosphere was prepared by the simple hydrothermal method. Subsequently, these $CoFe_2O_4$ nanospheres were dispersed in a glucose solutio, where the glucose molecules are attached to the surface of $CoFe_2O_4$ nanosphere via a hydrogen bond. During carbonization, the glucose molecules are decomposed to form a uniform thin layer of carbon on $CoFe_2O_4$ nanosphere [21]. As reported above, the fabricated $CoFe_2O_4$ nanoparticles have size-dependence on the ratio of carbon coating where the higher the ratio of glucose is used, the thicker the coating of carbon will be. However, at a maximum ratio of (2 : 1), the thickness of carbon coating decreases due to the saturated concentration of carbon.

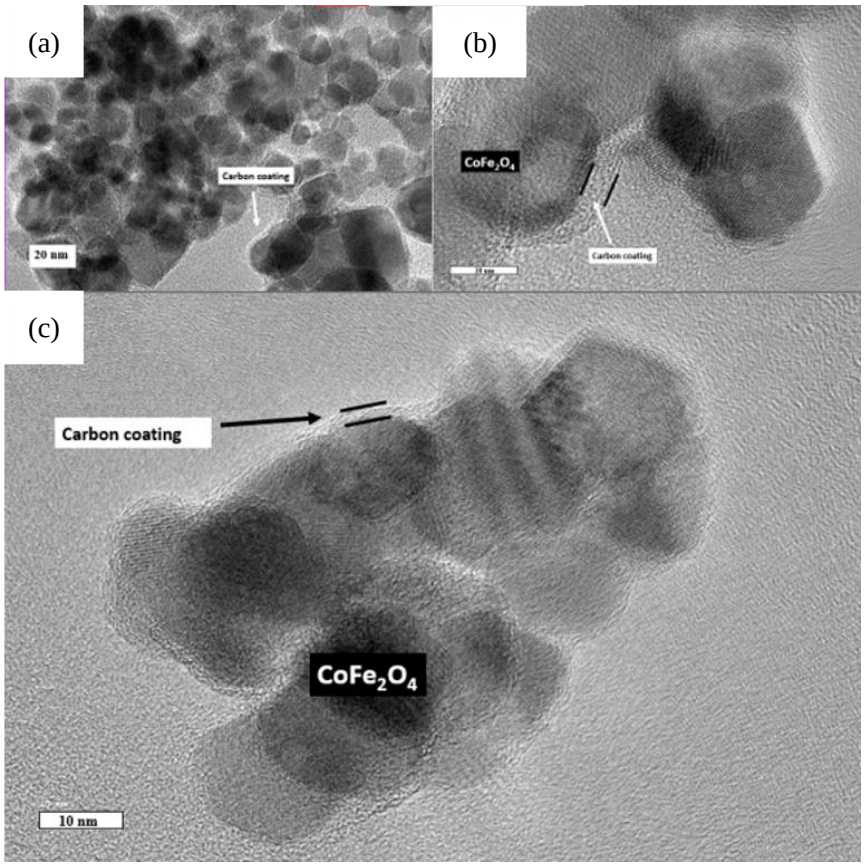

Figure 6. HRTEM images of carbon-coated $CoFe_2O_4$ samples at ratio (a) 1 : 1, (b) 2 : 1 and (c) 3 : 1.

4.5. Shielding Effectiveness

Figure 7 shows the total shielding effectiveness of carbon-coated $CoFe_2O_4$/epoxy nanocomposite at different ratios of carbon coating against X-band frequency. It can be observed that the curves are in wavy form due to the electromagnetic wave in the alternative current waveform having constant changes in its polarity in every half-cycle alternating between a positive maximum value and a negative maximum value accordingly to time [22]. The total electromagnetic shielding effectiveness of carbon coating at 2 : 1 within 10–11 GHz shows the higher value approximately 17 dB than other samples. In relating the structural analysis of the nanoparticle, it can be observed that the thicker the carbon coating is, the higher the SE value is. In addition, from the FESEM analysis also, it can be said that the fine dispersion and distribution of the $CoFe_2O_4$ nanoparticles in the polymer matrix result in informing interconnected conducting networks. The entering power signal interacts with the conductive network formed by the composite and helps in the movement of the electrons for the absorption of the incident wave [23].

The wavy curves in the graph are caused by the electromagnetic wave in the alternating current waveform. The wave has a constant change in polarity, alternating between a positive maximum value and a negative maximum value in every half cycle. The total electromagnetic shielding effectiveness (SE) of carbon coating at a thickness ratio of 2 : 1 within the frequency range of 10 to 11 GHz is approximately 17 dB, which is the highest value compared to the other sample. The SE value increases with the thickness of the carbon coating. This is because the carbon coating forms a conductive network that absorbs the incident electromagnetic wave. The thicker the carbon coating is, the more conductive the network becomes, and the more effectively it absorbs the incident wave. The fine dispersion and distribution of the $CoFe_2O_4$ nanoparticles in the polymer matrix also contribute to the high SE value.

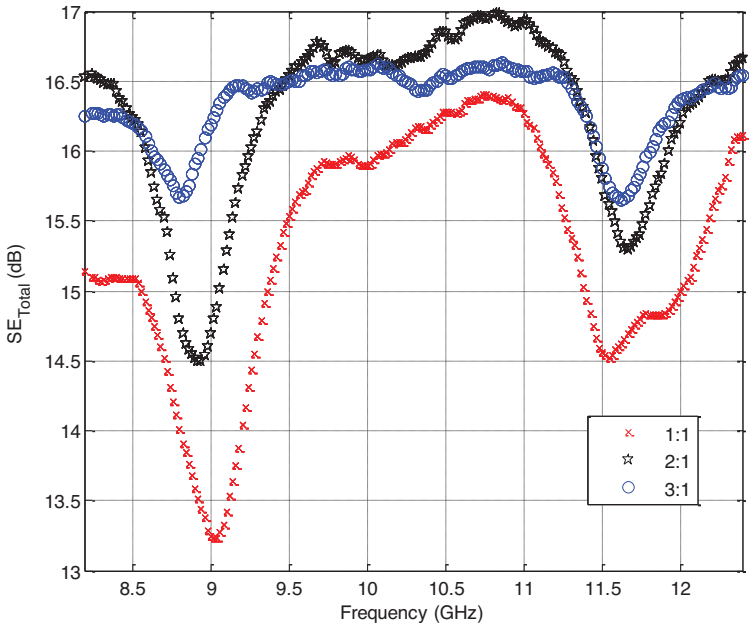

Figure 7. Total shielding effectiveness (SE_{total}) as a function of frequency measured in the X-band frequency of 8.2–12.4 GHz range of 3 different ratios of carbon coating.

The nanoparticles form interconnected conducting networks that interact with the entering power signa. This interaction helps to move the electrons in the network, which absorbs the incident wave. Overall, the results of this study show that carbon-coated $CoFe_2O_4$ nanoparticles/polymer composites are effective electromagnetic shielding material. The SE value can be increased by increasing the thickness of the carbon coating and by ensuring that the nanoparticles are well dispersed in the polymer matrix.

5. SUMMARY

We have succeeded in synthesizing spinel $CoFe_2O_4$ nanoparticles by a hydrothermal method utilizing only cobalt nitrate and iron nitrates as precursors and glucose as the carbon coating. Particle sizes of 11.47 nm were obtained at uncoated $CoFe_2O_4$ nanoparticles and 14.15 nm for the average of coated nanoparticles $CoFe_2O_4$. As the carbon coating increases, the particle size and carbon thickness increase at the maximum of ratio 2 : 1, and the shielding effectiveness is also at the highest and starts decreasing onwards. The sample is said to be at the optimum carbon ratio of 2 : 1. This simple, cost-effective, and environmentally friendly method that produces no by-product effluents can be used to synthesize pure crystalline spinel $CoFe_2O_4$ and carbon-coated $CoFe_2O_4$/epoxy nanocomposite. Furthermore, it can be extended to synthesizing other spinel ferrite nanoparticles of interest in nanotechnology in the application of electromagnetic shielding.

ACKNOWLEDGMENT

The authors would like to thank the Ministry of Higher Education for providing financial support under Fundamental Research Grant Scheme (FRGS) No. FRGS/1/2018/TK05/UMP/02/4 (University reference RDU190125) and UMP internal grant (RDU1803140 and PGRS200332).

REFERENCES

1. Wang, G., Y. Ma, Z. Wei, and M. Qi, "Development of multifunctional cobalt ferrite/graphene oxide nanocomposites for magnetic resonance imaging and controlled drug delivery," *Chemical Engineering Journal*, Vol. 289, 150–160, 2016, https://doi.org/10.1016/j.cej.2015.12.072.

2. Yahya, N., M. Kashif, N. Nasir, M. N. Akhtar, and N. M. Yusof, "Cobalt ferrite nanoparticles: An innovative approach for enhanced oil recovery application," *Journal of Nano Research*, Vol. 17, 115–126, 2012, https://doi.org/10.4028/www.scientific.net/JNanoR.17.115.
3. Senthil, V. P., J. Gajendiran, S. G. Raj, T. Shanmugavel, G. Ramesh Kumar, and C. Parthasaradhi Reddy, "Study of structural and magnetic properties of cobalt ferrite ($CoFe_2O_4$) nanostructures," *Chemical Physics Letters*, Vol. 695, 19–23, 2018, https://doi.org/10.1016/j.cplett.2018.01.057.
4. Žalnėravičius, R., A. Paškevičius, M. Kurtinaitiene, and A. Jagminas, "Size-dependent antimicrobial properties of the cobalt ferrite nanoparticles," *Journal of Nanoparticle Research*, Vol. 18, No. 10, 2016, https://doi.org/10.1007/s11051-016-3612-x.
5. Ju, Y. W., J. H. Park, H. R. Jung, S. J. Cho, and W. J. Lee, "Fabrication and characterization of cobalt ferrite ($CoFe_2O_4$) nanofibers by electrospinning," *Materials Science and Engineering B: Solid-State Materials for Advanced Technology*, Vol. 147, No. 1, 7–12, 2008, https://doi.org/10.1016/j.mseb.2007.10.018.
6. Wang, T., Z. Jiang, T. An, G. Li, H. Zhao, and P. K. Wong, "Enhanced visible-light-driven photocatalytic bacterial inactivation by ultrathin carbon-coated magnetic cobalt ferrite nanoparticles," *Environmental Science and Technology*, Vol. 52, No. 8, 4774–4784, 2018, https://doi.org/10.1021/acs.est.7b06537.
7. Souques, M., *Electromagnetic Fields, Environment and Health*, A. Perrin, ed., Springer International Publishing, 2012, https://doi.org/DOI 10.1007/978-2-8178-0363-0.
8. Zaroushani, V., A. Khavanin, S. B. Mortazavi, and A. Jonidi Jafari, "Efficacy of net epoxy resin for electromagnetic shielding in X-band frequency range," *Health Scope*, Vol. 5, No. 3, 2016, https://doi.org/10.17795/jhealthscope-30203.
9. Jusoh, M. A., Y. K. Yeow, R. Nazlan, and F. Esa, "Electromagnetic shielding effectiveness of gypsum-magnetite composite at X-band frequency," *Progress In Electromagnetics Research Letters*, Vol. 86, 21–26, 2019.
10. Liu, X., X. Yin, L. Kong, et al., "Fabrication and electromagnetic interference shielding effectiveness of carbon nanotube reinforced carbon fiber/pyrolytic carbon composites," *Carbon*, Vol. 68, 501–510, 2014.
11. Goodarz Naseri, M., E. B. Saion, H. Abbastabar Ahangar, A. H. Shaari, and M. Hashim, "Simple synthesis and characterization of cobalt ferrite nanoparticles by a thermal treatment method," *Journal of Nanomaterials*, 2010, https://doi.org/10.1155/2010/907686.
12. Vinila, V. S., R. Jacob, A. Mony, H. G. Nair, S. Issac, S. Rajan, A. S. Nair, D. J. Satheesh, and J. Isac, "X-ray diffraction analysis of nano crystalline ceramic $PbBaTiO_3$," *Crystal Structure Theory and Applications*, Vol. 3, No. 3, 57–65, September 2014, doi: 10.4236/csta.2014.33007.
13. Allaedini, G., S. M. Tasirin, and P. Aminayi, "Magnetic properties of cobalt ferrite synthesized by hydrothermal method," *International Nano Letters*, Vol. 5, No. 4, 183–186, 2015, https://doi.org/10.1007/s40089-015-0153-8.
14. Bohara, R. A., N. D. Thorat, M. Yadav, and S. H. Pawar, "One-step synthesis of uniform and biocompatible amine functionalized cobalt ferrite nanoparticles: A potential carrier for biomedical applications," *New Journal of Chemistry*, No. 7, 2979–2986, 2014, https://doi.org/10.1039/c4nj00344f.
15. Zhao, L., H. Zhang, Y. Xing, S. Song, S. Yu, W. Shi, X. Guo, J. Yang, Y. Lei, and F. Cao, "Studies on the magnetism of cobalt ferrite nanocrystals synthesized by hydrothermal method," *Journal of Solid State Chemistry*, Vol. 181, No. 2, 245–252, 2008, https://doi.org/10.1016/j.jssc.2007.10.034.
16. Sanpo, N., J. Wang, and C. C. Berndt, "Influence of chelating agents on the microstructure and antibacterial property of cobalt ferrite nanopowders," *Journal of the Australian Ceramic Society*, Vol. 49, No. 1, 84–91, 2013.
17. Brabers, V., "Infrared spectra of cubic and tetragonal manganese ferrites," *Phys. Status Solidi*, Vol. 33, No. 2, 563–572, 2010.
18. Farid, M. T., I. Ahmad, S. Aman, M. Kanwal, G. Murtaza, I. Ali, I. Ahmad, and M. Ishfaq, "SEM, FTIR and dielectric properties of cobalt substituted spinel ferrites," *Journal of Ovonic Research*, Vol. 11, No. 1, 1–10, 2015.

19. Issa, B., I. M. Obaidat, B. A. Albiss, and Y. Haik, "Magnetic nanoparticles: Surface effects and properties related to biomedicine applications," *International Journal of Molecular Sciences*, 21266–21305, 2013, https://doi.org/10.3390/ijms141121266.
20. Houshiar, M., F. Zebhi, Z. J. Razi, A. Alidoust, and Z. Askari, "Synthesis of cobalt ferrite ($CoFe_2O_4$) nanoparticles using combustion, coprecipitation, and precipitation methods: A comparison study of size, structural, and magnetic properties," *Journal of Magnetism and Magnetic Materials*, Vol. 371, 43–48, 2014, https://doi.org/10.1016/j.jmmm.2014.06.059.
21. Sankar, K. V., S. Shanmugapriya, S. Surendran, S. C. Jun, and R. K. Selvan, "Facile hydrothermal synthesis of carbon-coated cobalt ferrite spherical nanoparticles as a potential negative electrode for flexible supercapattery," *Journal of Colloid and Interface Science*, Vol. 513, 480–488, 2018, https://doi.org/10.1016/j.jcis.2017.11.054.
22. Qureshi, A., A. Mergen, and B. Aktaş, "Dielectric and magnetic properties of YIG/PMMA nanocomposites," *Journal of Physics: Conference Series*, Vol. 153, 2009, https://doi.org/10.1088/1742-6596/153/1/012061.
23. Chhetri, S., P. Samanta, N. C. Murmu, S. K. Srivastava, and T. Kuila, "Electromagnetic interference shielding and thermal properties of noncovalently functionalized reduced graphene oxide/epoxy composites," *AIMS Materials Science*, Vol. 4, No. 1, 61–74, 2017, https://doi.org/10.3934/matersci.2017.1.61.